A DIFFUSION TENSOR IMAGING STUDY OF AGE-RELATED CHANGES IN THE WHITE MATTER STRUCTURAL INTEGRITY IN A COMMON CHIMPANZEE

A Thesis
Presented to
The Academic Faculty

by

Bhargav Kumar Errangi

In Partial Fulfillment
of the Requirements for the Degree
in the
Department of BioMedical Engineering

Georgia Institute of Technology
May, 2009

A DIFFUSION TENSOR IMAGING STUDY OF AGE-RELATED CHANGES IN THE WHITE MATTER STRUCTURAL INTEGRITY IN A COMMON CHIMPANZEE

Approved by:

Professor Xiaoping Hu, Committee Chair
Department of BioMedical Engineering
Georgia Institute of Technology

Professor James.K.Rilling, Advisor
Department of Anthropology
Emory University

Professor Todd.M.Preuss
Division of Neuroscience
Yerkes National Primate Research Center

Professor Shella Keilholz
Department of BioMedical Engineering
Georgia Institute of Technology

Date Approved: November 17, 2008

ACKNOWLEDGEMENTS

First, I would like to thank my advisor, Dr. James.K.Rilling, for giving me an oppurtunity to be a part of his group. I will always be grateful for his valuable advice, insight, guidance and constant support. I would also like to extend my gratitude to the Masters defense committee: Dr. Xiaoping Hu , Dr. Todd Preuss and Dr.Shella keilholz. I appreciate their time and effort in serving on my committee.

I would like to thank Matt Glasser,Dr.Longchuan Li for their valuable help and constant support throughout the project. Also, I would like to thank all the members of the Laboratory of darwinian neuroscience for their support and encouragement.

TABLE OF CONTENTS

LIST OF FIGURES

CHAPTER I

INTRODUCTION

Diffusion-Tensor Magnetic Resonance Imaging (DTI) reveals the orientation of white matter fiber tracts in vivo and yields an index of brain white matter micro structural integrity through quantification of the directionality of water diffusion. Fractional Anisotropy (FA), a measure derived from the diffusion tensor data, is sensitive to developmental and pathological changes in axonal density, myelination, size and coherence of organization of fibers within a voxel. (Basser et al 1995; Pierpaoli C et al 1996; Beaulieu et al .2002) It therefore reflects the structural integrity of white matter. There is substantial evidence that brain white matter structural integrity decreases with age in humans .Several DTI studies reported the decline in white matter structural integrity in humans during normal aging (Pfefferbaum and Sullivan,2003; Pfefferbaum et al., 2000a; O'Sullivan et al., 2001; Chun et al., 2000; Nusbaum et al., 2001; Stebbins et al.,2001; Madden et al., 2004.). This decline is observed in both men and women, and is linear from about age 20 years onwards. There is less evidence about the pattern of normal aging in chimpanzees, our closest living primate relative. Very few studies have compared brain aging in humans and chimpanzees. Comparing age-related brain structure changes in humans and chimpanzees would define a human-specific pattern of normal aging and would be a proper background for interpreting observed changes in the neurodegenerative diseases of the elderly beyond those of normal aging. A number of methods have been proposed to describe age-related changes in white matter structural integrity using DTI metrics. In this project, Regions of Interest (ROI) analysis and Tract Based Spatial Statistics (TBSS) are used to describe the age-related changes in chimpanzees. Strengths and

limitations of these methods are discussed.

1.1 Background

1.1.1 Diffusion Tensor Imaging (DTI)

Diffusion is a physical process that involves the translational movement of molecules via thermally driven random motions, called Brownian motion. When there are no hindrances to diffusion, the amount of diffusion is same in all the directions and is termed as isotropic diffusion. However, if there are barriers to diffusion, such as white matter axons, and diffusion is preferred in some directions over others; it is termed as anisotropic diffusion. The mobility of all the water molecules can be characterized by a diffusion coefficient.

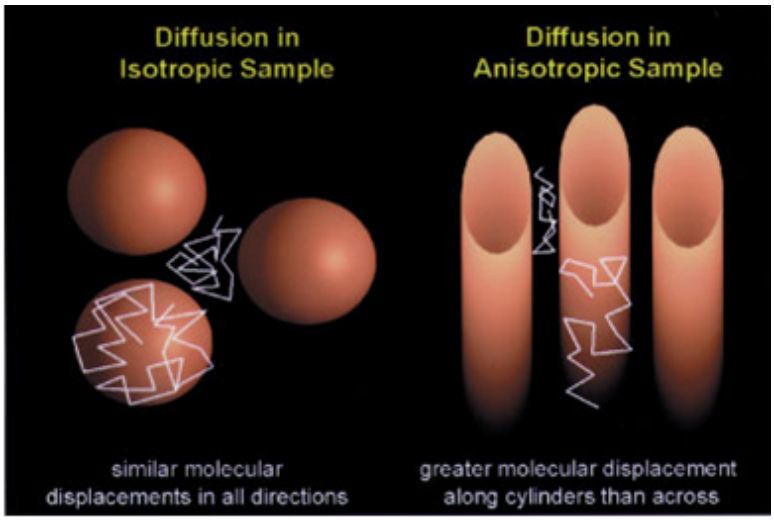

Figure 1: Figure showing the molecular displacements in isotropic and anisotropic media. Displacements are similar in all directions for isotropic sample and oriented more along the axis in an anisotropic sample.

Magnetic resonance measurements of diffusion are sensitive to the displacement of the molecules along the axis of the diffusion-sensitizing gradients that are applied. Therefore, diffusion along different directions can be readily measured by changing the direction of the diffusion sensitizing gradients. The effect of diffusion on MRI signal is attenuation(s). This attenuation depends upon the diffusion coefficient, D

and on the b, which characterizes the strength and duration of diffusion-sensitizing gradients applied. This relationship is given by,

$$Signal(S) = exp(-bD) \tag{1}$$

The contrast in diffusion-weighted images is dependent on the diffusive mobility of the tissue under study. For the same degree of diffusion weighting, the signal from free water or cerebrospinal fluid (CSF) will be highly attenuated compared to the signal from the restricted water in the tissue compartments.

In the presence of anisotropy, diffusion can no longer be characterized by a single scalar coefficient but requires a tensor, D, which fully describes molecular mobility along each direction and correlation between these directions. The diffusion tensor D is symmetric and is given by,

$$\bar{D} = \begin{matrix} D_{xx} & D_{xy} & D_{xz} \\ D_{yx} & D_{yy} & D_{yz} \\ D_{zx} & D_{zy} & D_{zz} \end{matrix}$$

Figure 2: Symmetric Diffusion Tensor

Signal attenuation not only depends on the diffusion effects measured along one direction of the diffusion sensitizing gradient pulse but may also include the contributions from the other directions. So in order to determine the diffusion tensor accurately, diffusion-weighted images have to be collected along several gradient directions. As the diffusion tensor is symmetric, measurements along at least six directions are necessary. In any anisotropic media, the diffusion tensor, its constituent principal diffusion directions, and principal diffusivities are estimated at each voxel. The former are mutually perpendicular, preferred directions along which molecular displacements of the molecules are uncorrelated, while the later are the diffusivities along these directions. These measures are also called Eigen values (principal diffusivities) and Eigen vectors (principal directions). The largest Eigen vector of the

tensor corresponds to the principal diffusion direction within a voxel.

Once the diffusion tensor and constituents are estimated, the amount of restriction to diffusion in an anisotropic media can be typically expressed as Fractional Anisotropy (FA) (Pierpaoli and Basser (1996)). FA is a measure of orientation coherence and is given by:

$$FA = \frac{\sqrt{3}}{\sqrt{2}} \frac{\sqrt{(\lambda_1 - \lambda)^2 + (\lambda_2 - \lambda)^2 + (\lambda_3 - \lambda)^2}}{\sqrt{\lambda_1^2 + \lambda_2^2 + \lambda_3^2}}$$

Figure 3: Fractional Anisotropy

The values of FA range from 0 to 1. In white matter the FA values are closer to 1 since the water diffusion is restricted by its fiber constituents, which are arranged in parallel. On the other hand, FA is near 0 in ventricular cerebrospinal fluid, where diffusion is isotropic. The average value of diffusion at a voxel is expressed as the Apparent Diffusion Coefficient (ADC), bulk Mean Diffusivity (MD), or trace of a tensor matrix. ADC is a quantitative metric of water motility (independent of the orientation) in a voxel and is commonly but not necessarily negatively correlated with FA.

1.1.2 DTI and Brain White Matter in Normal Adult Aging

Diffusion in brain white matter is present in two principal compartments: the extracellular space and intracellular space. Water diffusion is anisotropic in the extracellular space due to ordered arrangement of the myelinated fibers. Interstitial fluid in spaces between the fibers provides the avenue for diffusion. Myelin, the axonal membrane, microtubules and neurofilaments are all longitudinally oriented structures (Figure4) that could hinder the water diffusion perpendicular to the length of the axon and result in orientational diffusion (basis for anisotropy). The amount of myelination,

the length and the numbers of fibers determine the degree of anisotropy in the extracellular space. These physical characteristics of white matter fibers change by region. In intracellular space, cytoplasm provides another medium for diffusion crowded with cytoskeletal constituents. In normal aging, disruption in the white matter microstructure can reflect the breakdown of myelin, constituents of cytoskeleton, axon density (Basser et al., 1995), length and number of myelinated fibers (Marner et al. 2003).

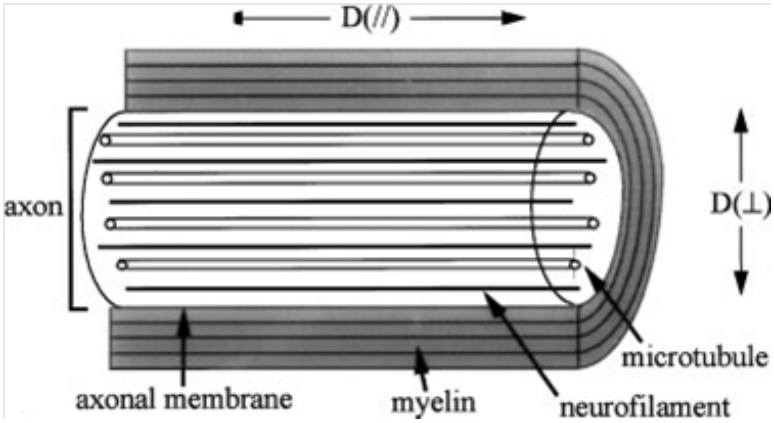

Figure 4: Figure explains the structural organization of a neuron forming the basis for anisotropic diffusion. The myelin, axonal membrane, microtubules, neurofilaments that constitute a neuron form a barrier for diffusion perpendicular to the length of the axon resulting in anisotropic diffusion.

Several structural neuroimaging studies have looked at changes in the brain volume with age. There is a consistent increase in the CSF-filled spaces that occur primarily at the expense of cortical gray matter during normal aging (Blatter et al. 1995). Macro structural, age-related volume reduction in brain white matter is small in the normal population (Sullivan et al. 2004). A few studies, however, report a greater white matter volume decline than gray matter (Guttmann et al. 1998), but such loss is typically small, around 2 percent per year, and accelerates in old age. Several studies reported that men have greater overall brain volume and a greater ratio of white matter to overall brain volume, compared with women (Sullivan et al 2004). The slope of change in white matter/gray matter volume is smaller for women than men. A cross-sectional study on a group of healthy adults (95 men and 48 women)

revealed an age-related decline in gray matter volume but not in white matter volume (Sullivan et al. 2004) (Figure5).

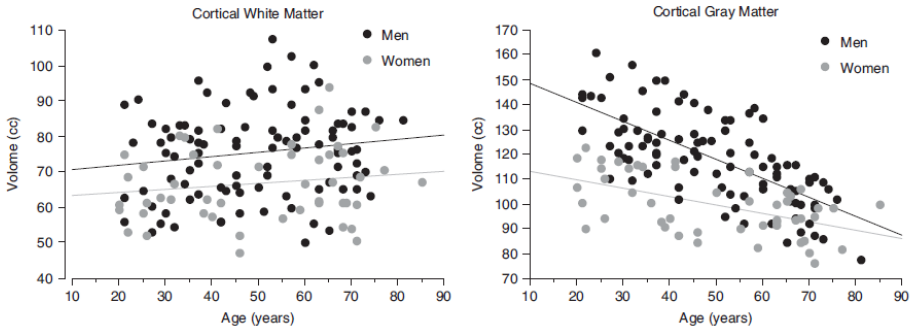

Figure 5: A cross-sectional study showing age-related decline in cortical gray but not white matter volumes in healthy adults (95 men and 48 women) (Sullivan et al. 2004)

White matter Fractional Anisotropy (FA), a measure derived from the DTI data is sensitive to developmental and pathological changes in the micro structural characteristics of the myelinated axons. Many studies often use the FA as an index of decreasing white matter health. Decline in FA offers insight into the degenerative changes in the micro-structural integrity of white matter tracts. Various degenerative disorders, such as multiple sclerosis, and various dementias show decline in the white matter FA (Horsfeild and Jones; 2002). Several DTI studies also reveal age-related declines in white matter FA in normal healthy adults (Pfferbaum and Sullivan 2003 Pfefferbaum et al., 2000a; O'Sullivan et al., 2001; Chun et al., 2000; Nusbaum et al., 2001; Stebbins et al.,2001; Madden et al., 2004;Salat et al., 2004; Head et al.). The FA decline with age was shown to be due to an increase in water diffusion in the direction perpendicular to the direction of the white matter fibers. This is caused by disruption of axonal myelin sheath (demyelination) and/or replacement of the axonal fibers with other cells (gliosis) (Maziootta et al, 1995). Disruption/damage to the cells is assumed to be mainly caused by certain highly reactive free radicals called as Reactive Oxygen Species (ROS), which are produced as byproducts of oxidative

metabolism. This process is also well known as oxidative stress (Beal et al. 1995).

Increased interstitial fluid within the white matter (e.g., leukoaraiosis) (Helenius et al., 2002)and partial volume effects resulting from inclusion of gray matter and/or CSF in the white matter sample influence the decline of anisotropy with age. Pfefferbaum et al. (2003) performed morphological erosion of white matter regions of interest to remove the inclusion of non-white matter pixels in the FA calculations. Reducing the size of the white matter samples attenuated but did not negate the effects. This indicates that the observed decrease in white matter FA with age reflects true micro-structural alterations, rather than sampling artifact. Another complicating factor is that intravoxel fiber incoherence (such as fiber crossing) decreases the FA measured at a particular voxel. Optimal choice of multiple gradient direction schemes are usually used to eliminate any intravoxel coherence effects. Deep white matter hyperintensities seen on t2-weighted images are likely to cause a significant decrease in the white matter FA. These hyperintensities are due to lesions within the white matter (leukoaraiosis) and influence the decline of anisotropy with aging as mentioned above.

White matter regions have different degrees of anisotropy, dependant on the homogeneity of the fiber structures. Thus, the corpus callosum should have a high FA because of the density of fibers oriented in a medio-lateral direction. On the other hand, the white matter tracts leading to the frontal lobes and pericallosal regions have low FA due to the crossing of the white matter tracts. Aging affects different white matter systems differently. It has been hypothesized that later-maturing structures are more vulnerable to the effects of aging compared to the early maturing structures (Raz et al.1993). Also, the amount of myelination and the diameter of the fibers increase the vulnerability to the effects of aging. In corpus callosum (CC), the decline in FA for the genu (anterior region of CC) is high compared to splenium (Posterior region of CC). Myelination of splenium precedes that of the genu (Rakic P et al. 1968),

possibly causing the later maturing anterior regions to show higher or earlier age-related declines than posterior regions. Also, genu is composed of a relatively large proportion of small diameter, lightly myelinated fibers. The structures showing the greatest FA declines over the age range of 23-76 years were in the genu of the corpus callosum and the centrum semiovale (Pfefferbaum et al. (2003)). Centrum semiovale is the region where many important tracts intermix, including the inter-hemispheric callosal projections, the superior longitudinal fasciculus, and the cortico-spinal tract. The Figure6 below shows the age-related changes in FA across the seven regions for 31 subjects (Pfefferbaum et al., 2003).

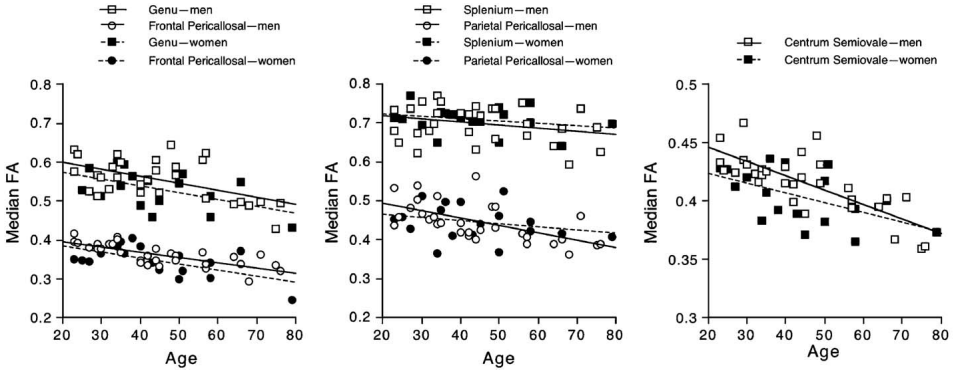

Figure 6: Healthy men and women showed equivalent and significant decreases in FA with advancing age, which was greater in the genu than the splenium and greatest in the centrum semiovale. Pfefferbaum et al. (2003).

Studies pertaining to age-related differences between men and women showed the same pattern of decline in white matter structural integrity (Sullivan et al. (2000)), involving greater age-dependant deterioration in frontal regions than in parietal regions. Kochunov et al. (2007) studied the relationship between FA and other indices of cerebral health like gray matter thickness, sulcal width and white matter hyper-intense volumes. Results showed a significant correlation between FA of the genu and gray matter thickness independent of the cortical area, while the FA of the other regions did not have any relationship with the gray matter thickness. Decreases in FA of the genu are strongly correlated with the sulcal span and the hyper-intensity

of white matter volume. This might suggest that changes in myelin levels in the thinly myelinated associative tracts of genu could be an indicator of overall decline in other indices of cerebral health. The corpus callosum (CC) displays heterotopic antero-posterior cortical connectivity. Furthermore, specific regions of the CC comprise fibers connecting hetero and unimodally associated cortical regions [Huang et al.2005; Witelson 1989]. The genu, rostral body, anterior midbody, posterior midbody, isthmus and splenium comprise fibers connecting caudal/orbital prefrontal areas and inferior premotor area, prefrontal area, frontal area and motor system, frontal area and motor system, parietal area, temporal and occipital areas, respectively, and the FA and MD values of CC sub regions are linked to the associated regions [Hasan et al. 2005; Ota et al.2006]. Evaluation of normal-appearing white matter of the CC sub regions could be used as a marker of the projection area, where ROIs are difficult to place.

1.1.3 Functional Correlates

DTI measures of white matter microstructure explain the brain structure-function relationships during normal aging, which have been difficult to establish using volumetric measures. A number of studies have examined the decline in white matter FA and its relationship with tests of cognitive and motor functions including working memory, attention shifting and other executive functions. For example, Sullivan et al. (2006) used an alternated finger tapping task as a measure of interhemispheric transfer and processing speed and correlated the output with the corpus callosum FA. Results showed that splenium FA and parietal pericallosal FA correlated significantly with the alternating task indicating that decline in corpus callosum micro-structural integrity influences efficiency in interhemispheric processing. Charlton et al. (2006) correlated the white matter FA and ADC values with results from the cognitive tests of executive function, working memory, and information-processing speed. After controlling

for age, DTI parameters correlated with results from the cognitive tests indicating age-related cognitive decline.

1.1.4 Brain Aging in Non-Human Primates

There is no substantial evidence explaining structural changes in the brain due to physiological aging in non-human primates. However, there are few studies that explain the brain size and volumetric changes in non-human primates. Postmortem analysis of brain weight in macaques, unlike humans, reveals no decline with from young to old adulthood (Herndon et al. 1998a). In addition to brain weight, there is at present no clear evidence from histological studies of major gray matter or white matter volume reductions with aging in nonhuman primates. Histological studies described the ballooning and splitting of myelin sheaths at the ultra structural level in aged macaques, and similar degenerative changes appear to occur in humans as well (Feldman and Peters, 1998; Peters et al., 2000; Peters and Sethares, 2002).

Herndon et al. 1999 calculated brain weights from 76 chimpanzees ranging in age from birth to 59.4 years of age. These results suggest that brain weight declines moderately (but not statistically significant) with age in the chimpanzee as it does in humans. Andersen et al. (1999), in cross-sectional studies of female macaque monkeys, reported there is significantly less gray matter volume (more than 10 percent less) in old monkeys (21-27 yrs) compared to young monkeys, but more ventricular and white matter volume. Lyons et al. (2004) also reported increased white matter in old versus young female squirrel monkeys, as well as a small, but nonsignificant, decline in gray matter. Macro structural volumetric studies conducted on rhesus macaques by Lacreuse et al., 2005 also suggests reductions in the volume of gray matter regions like caudate and putamen with age. Pierre et al. (2008) looked at age-related differences in gray and white matter ratio, total brain volume, and corpus callosum morphology in bonnet macaques ranging in from juvenile to adult. The

finding of higher gray and white matter in juvenile as compared to adolescent and adult monkeys parallels similar decreases in gray matter volumes in humans.

There are no published DTI studies that describe the age-related changes in white matter microstructure in the non-human primates, especially chimpanzees. The current evidence for chimpanzees, suggests no age-related loss of white matter volume, and possibly even an increase, contrary to the very clear evidence for age-related white matter volume reduction in humans (Sullivan et al. 2004). Comparing the age-related changes in the white matter integrity both micro structurally and macro structurally of humans with chimpanzees would define a human-specific pattern of normal aging and would be a proper background for interpreting observed changes in the neurodegenerative diseases of the elderly beyond those of normal aging.

CHAPTER II

IMAGE ACQUISITION AND PRE-PROCESSING

2.1 Echo Planar Imaging

Echo Planar Imaging (EPI) is one of the most commonly used magnetic resonance imaging sequences for acquiring diffusion weighted images. Diffusion is the random thermal motion of molecules through a tissue compartment. The signal intensity of Magnetic Resonance Imaging is dependent on water motion among other factors, which intrinsically produces contrast. In diffusion-weighted echo-planar imaging, image acquisition is sensitized to the diffusion of water molecules by inserting very strong motion-sensitizing gradient pulses into the echo-planar imaging pulse sequence.

2.1.1 Principle

In Echo Planar Imaging (EPI), all the k-space lines are acquired within a single repetition (i.e. the complete image is acquired from one single free induction decay signal around 40 to 100 ms in duration of a gradient echo or spin echo sequence). Similar to a conventional Spin Echo sequence, a Spin Echo based echo planar imaging sequence begins with 90 and 180 RF pulses. However, after the 180 RF pulse, the frequency-encoding gradient oscillates rapidly from a positive to negative amplitude, forming a train of echoes . Since the complete image is acquired within a single repetition it is called as a single-shot sequence. On the other hand, if all the data points required to make-up an image are acquired in several free induction decays, it is called a multi-shot EPI or interleaved EPI. This technique is sometimes referred to as segmented EPI, since the data points are acquired by dividing the k-space into two or more segments.

For example, in a two shot EPI, the first interleave covers the whole of k-space

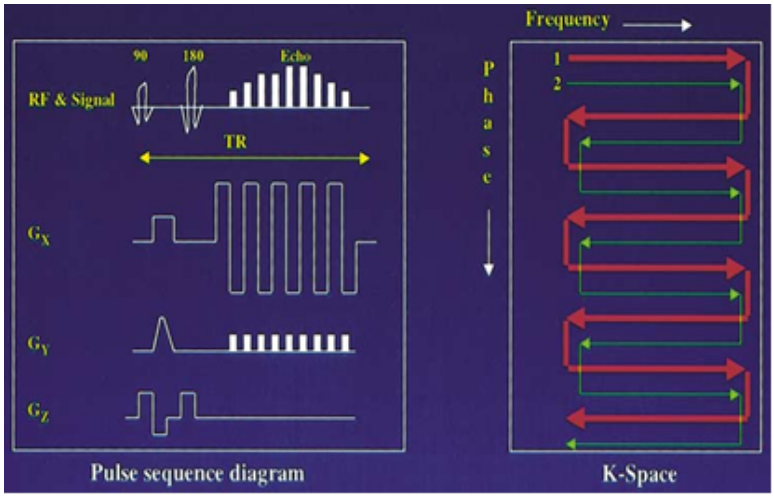

Figure 7: Pulse sequence diagram and k-space traversal of a single shot EPI sequence

in alternate lines, and then the second pass fills in the lines between (Figure8). The same principle is extended to any number of interleaves.

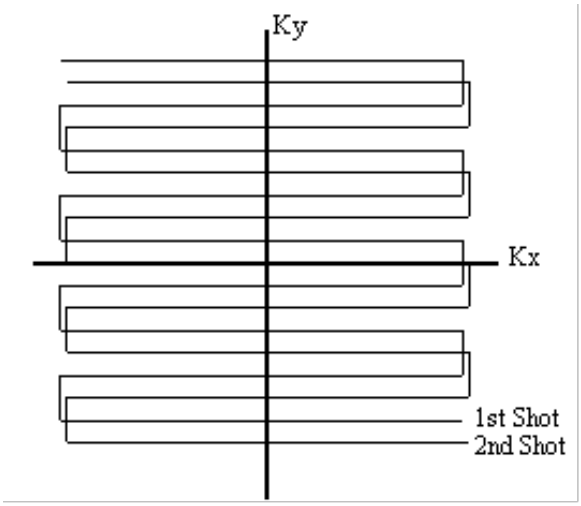

Figure 8: K-space traversal in a two-shot Echo planar Imaging. The first interleave covers the whole of k-space in alternate lines, and then the second pass fills in the lines between.

2.2 Echo Planar Diffusion Weighted Imaging in Chimpanzees

In Single Shot EPI only one excitation is necessary to acquire an image and hence, the DWI images become less sensitive to subject motion, but extremely sensitive to small deviations in the magnetic field. One of the most serious problems of EPI is caused

by field inhomogeneity. Field inhomogenities can be caused by imperfections within the magnet, eddy-current induced local gradients, and magnetic susceptibility effects caused by the sample, especially near the air-tissue interfaces. The variations in the field cause the signals to resonate at different frequencies. The effects are less severe along the readout direction in EPI due to the usage of large gradients. However, along the phase encode direction, the off-resonance effects are more severe resulting in a considerable shift in pixel position. This in turn causes spatial distortion of the images. These effects are exaggerated at higher field strengths. In chimpanzees, due to complicated sinus anatomy and large air-tissue interfaces the spatial distortion caused by magnetic susceptibilities is severe (Figure9).

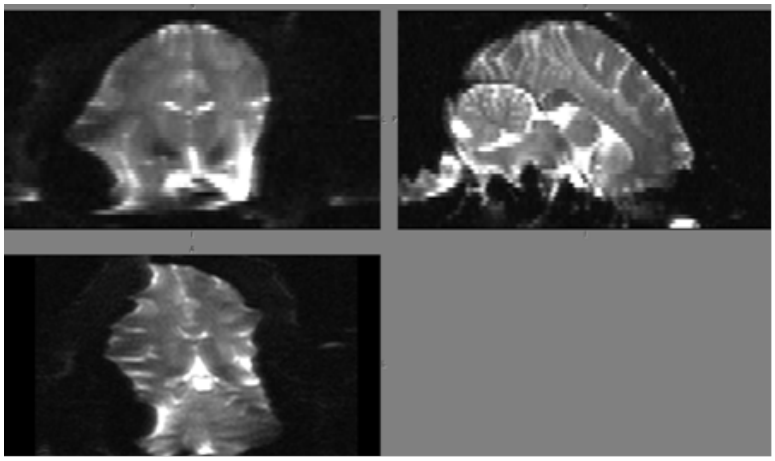

Figure 9: Large Geometric distortions caused by the magnetic susceptibility artifact at the air-tissue interfaces using single-shot EPI sequence in chimpanzees. Figure shown is a b0(no diffusion weighting) image.

Moving from single shot imaging to multi-shot EPI imaging reduces the extent of spatial distortion due to increases in the number of excitations needed to acquire the information from one slice. Therefore, the off- resonance errors, resulting from field inhomogeneity and susceptibility, which evolve constantly with time are significantly reduced. The type of sequence and the method used for correcting the spatial distortion in segmented EPI is discussed in the Image Acquisition section. However, a potential drawback of multi-shot EPI is that it increases the scan time by n fold,

where n is the number of shots or segments used in the sequence. However, while segmented EPI is often used to reduce the spatial distortions (figure 4) and increase the spatial resolution, it also increases the susceptibility to brain motion.

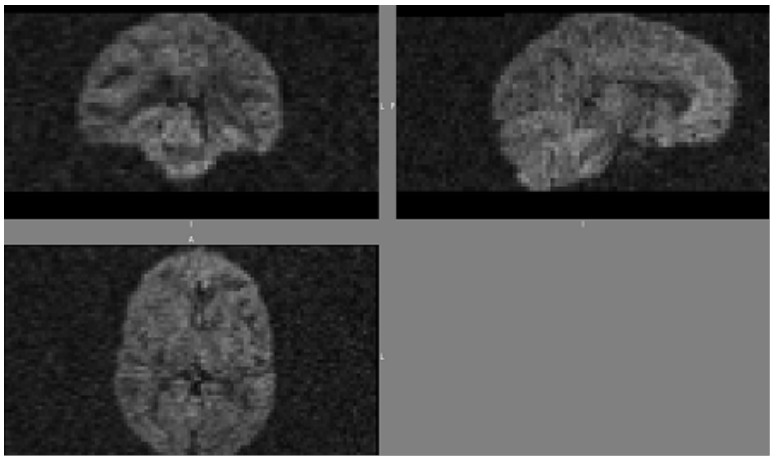

Figure 10: Significantly reduced geometric distortions using segmented EPI sequence (4 segments) compared to single shot EPI in chimpanzees. One of the diffusion weighted volumes is shown in the figure.

Subject motion in segmented EPI causes small incoherent phase changes between the segments, leading to severe image artifacts. These artifacts are often referred to as ghosts in an image. The main source of this type of ghosting is cardiac pulsation with occasional involuntary movement of the subject. This is one of the potential problems of segmented EPI acquisition. Even the use of cardiac gating to synchronize the data acquisitions in combination with simple readout navigator echo approach cannot suppress all motion related phase errors. As a result residual artifacts are often found in the corrected images. There will be loss of signal within the brain due to ghosting, which results in poor SNR and inaccurate estimation of the diffusion metrics like Fractional Anisotropy (FA) from the diffusion weighted images. Figure11 illustrates the ghosting artifact in chimpanzee DTI data acquired using segmented EPI sequence.

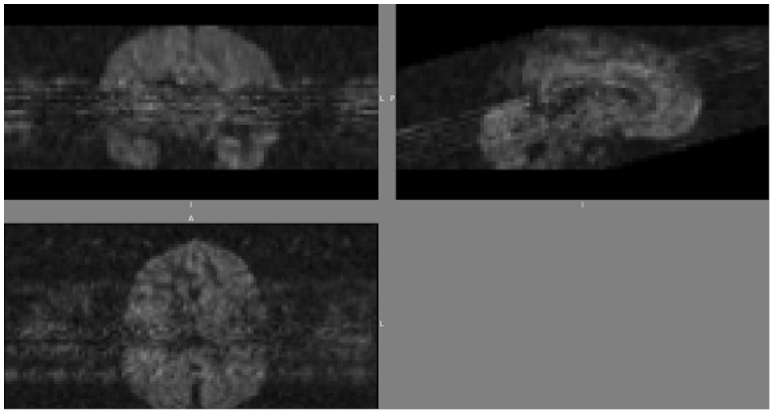

Figure 11: Figure shows increased motion artifact in chimpanzees using segmented EPI. Ghosts appear in the image as streak of lines covering a range of slices. Ghosting in one of the diffusion weighted volumes is shown in the figure.

2.3 Image Acquisition

Three groups of healthy, female chimpanzees were studied: 9 Younger (Mean=14.1, SD= 2.1), 7 old (Mean=35.8, SD=3.02) and 5 very old (Mean=50.4, SD=2.5). A four shot echo-planar double spin echo, T2-weighted sequence was used to acquire diffusion-weighted data with a spatial resolution of 1.8mm isotropic (FOV 230mm, matrix 128x128). The sequence parameters were TE/TR/Slices= 91ms/5740ms/41, with 60 diffusion-weighted directions and two diffusion weighting b values of 0 and 1000. Two averages, one with bottom-up and one with top-down (Bowtell et al (1994)) traversal of k-space in the phase-encode direction, were acquired. The method for distortion correction due to magnetic susceptibilities in segmented DTI acquisitions proposed by Andersson et al. (2003) can be used on the images acquired using a phase up and phase down approach. Diffusion contrast increases with increase in the gradient strength and number of diffusion gradient directions, so acquiring DWI images along 60 directions with a b value of 1000 would increase the contrast compared to fewer directions and a low b value and will result in better quantification of diffusion metrics. The number of measurements of Signal from the b0 and the diffusion weighted images affect the calculation of the diffusion tensor and the measured DTI

metrics. According to D.K. Jones et al (1999) optimal ratio between numbers of measurements without diffusion weighting to the measurements with diffusion weighting to yield a less variant and precise diffusion tensor matrix is 8.3:1. Based on that assumption, five b0's were acquired for each average of the diffusion weighted images. Total scan time per acquisition was around 24 minutes.

2.4 Image Pre-processing

2.4.1 Motion Correction

Segmented EPI increases the susceptibility to motion compared to single shot EPI. Simple head motion was corrected by registering all the 60 diffusion weighted volumes to the b0 image (Reference image). Rigid body registration with six degrees of freedom was used for the registration.

2.4.2 Eddy Current Correction

Rapidly switched gradients induce eddy currents in conductive materials resulting in a residual eddy current field (ECF). These residual eddy currents cause image shearing, scaling and bulk shifting in the diffusion weighted images The problem of residual ECF's is even more complicated in EPI experiments involving multiple gradient pulses. The magnitude of the eddy current field depends on the direction and strength of the applied diffusion sensitizing field gradients. The values of these applied diffusion gradients differ for different diffusion weighted directions. These distortions were corrected, using affine registration with six degrees of freedom to a reference volume, in this case a b0 image

2.4.3 Distortion Correction

Geometric distortion due to magnetic susceptibilities is severe in chimpanzees due to complicated sinus anatomy and large air-tissue interfaces. Magnetic susceptibility distortion correction was performed using the method proposed by Andersson et al.

(2003). Using the two diffusion weighted averages, one with bottom-up and the other with top-down Bowtell et. al (1994) traversal of k-space in the phase-encode direction. This results in two images with identical magnitude distortions in opposing directions. A displacement field was estimated from the two distorted images. The displacement field contains information about the signal which differs in the two acquisitions only with respect to the effects of susceptibility of the induced field inhomogenities. This displacement field was applied for each diffusion direction to restore the images to its undistorted state using least squares approach. These can be combined for each acquisition and the two acquisitions are averaged to yield an undistorted, averaged diffusion weighted image. Averaging improves the signal-to-noise ratio of the diffusion weighted volumes. This correction is very important for the estimation of a distortion-free diffusion tensor map.

2.5 Diffusion Tensor Estimation

This step involves the fitting of a local model of diffusion to the diffusion weighted data obtained after eddy current and susceptibility induced distortion correction at each voxel. Dtifit, a part of FDT (FMRIB's Diffusion Toolbox) was used for fitting the diffusion tensor model at each voxel. Dtifit uses the brain extracted mask of the b0 image, gradient vectors and gradient strength values for all the diffusion weighted directions to estimate the diffusion tensor. The gradient directions are rotated relative to the subject's position in the scanner before running dtifit. The output of the dtifit include the Eigen value maps, which give the amount of diffusion in the three orthogonal directions at each voxel, the Eigen vector maps, which describe the direction of diffusion corresponding to each eigen value, a Fractional Anisotropy map which is a measure of directionality of diffusion, a Apparent Diffusion Coefficient map, which gives the average value of diffusion at each voxel, and a raw T2 signal map without diffusion weighting.

2.6 Region Of Interest(ROI) analysis

One of the measures most commonly derived from diffusion data is fractional anisotropy (FA), which quantifies the strength of the directionality of the local tract structure. The FA values from the regions of interest (ROI) defined within the white matter provide information about white matter structural integrity during development and disease. In humans, white matter FA values decrease with age. To observe the trend of change in white matter structural integrity with age, regions of interest were defined within the white matter, more specifically the corpus callosum which is the largest white matter fiber bundle in the brain. The corpus callosum is divided into seven different segments based on Witelson‘s procedure (Witelson et al. 1989 Figure12). The seven different segments are (from anterior to posterior) rostrum, genu, rostral body, anterior mid body, posterior mid body, isthmus and splenium. According to Witelson‘s procedure, the seven different segments were defined along the horizontal line joining the farthest ends of corpus callosum. For example, the splenium is defined as one-fifth of the total distance along the horizontal line from the posterior end of the corpus callosum

ROIs based on the Witelson procedure were defined on mid sagittal slices of the T1-weighted images (Figure13 and Figure14). T1-weighted images provide good contrast between the white matter and gray matter within the brain and are very useful in defining the anatomical regions of interest. In most of the cases, the longest line joining both the ends of corpus callosum is not horizontal in the mid-sagittal plane due to inaccuracy in aligning the slices parallel to the corpus callosum during acquisition. Hence, we need to rotate the mid-sagittal images so that Witelson‘s convention of drawing the ROIs can be used. The structural images are rotated using NUDGE (FMRIB‘S rotation tool). The rotation and translation parameters provided to the Nudge are based on different trials and visual inspection of the alignment.

In the next step, the partial volume maps of white matter, gray matter and CSF

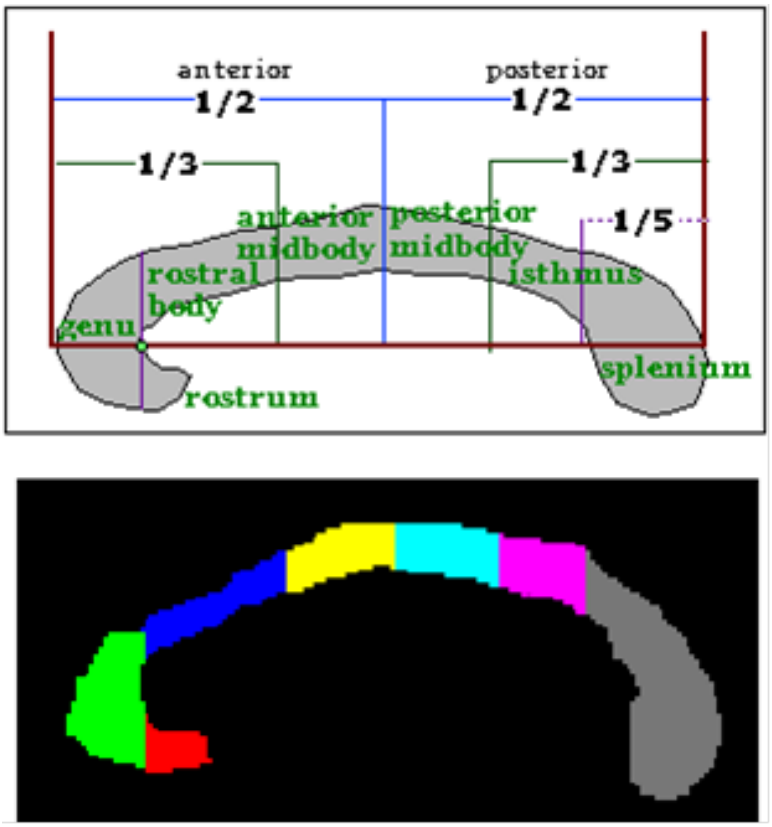

Figure 12: Witelson's convention of drawing the ROIs in the corpus callosum. ROIs of seven different regions of corpus callosum overlayed on it are also shown.

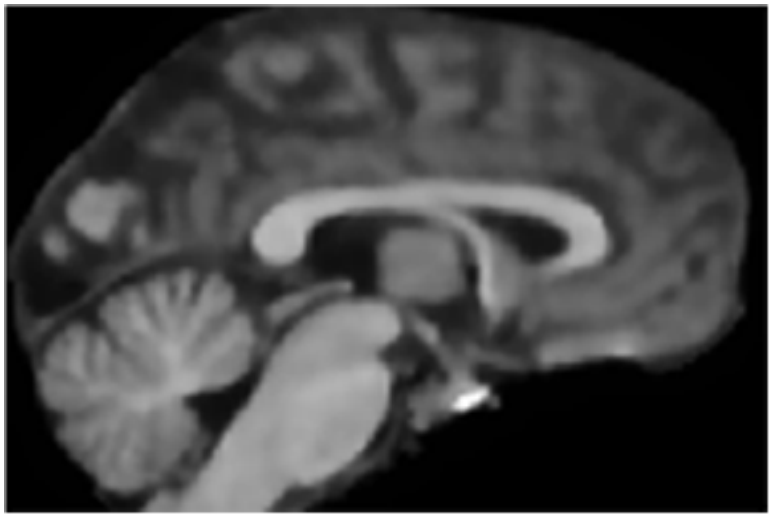

Figure 13: Rotated structural image using NUDGE (FMRIB'S rotation tool)

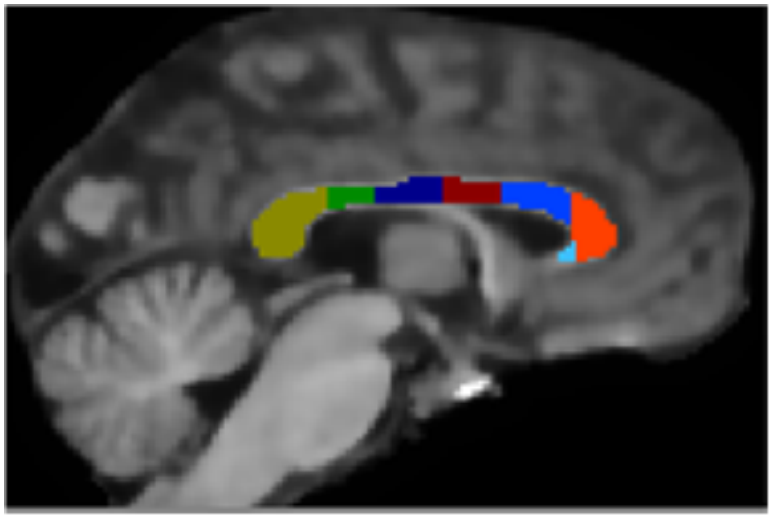

Figure 14: Corpus callosum ROIs overlayed on the structural image following the witelson convention

are obtained from the structural images. These maps are obtained using FAST (FMRIB'S automated segmentation tool; http://www.fmrib.ox.ac.uk/fsl/fast4/index.html) (Zhang et al. 2001). The partial volume maps are calculated based on the percentage of the tissue within each voxel. The seven different segments of the corpus callosum are manually defined on the structural images following the Witelson convention. Once the partial volume maps are obtained, the white matter map is transformed into the DTI space (using FA map as the reference image) using FLIRT (FMRIB'S automated registration tool; http://www.fmrib.ox.ac.uk/analysis/research/flirt/) (Jenkinson et al. 2001). Rigid body registration with six degrees of freedom is used. A sinc interpolation with a hanning window with a width of seven voxels is used for interpolation.

This white matter map is thresholded using a white matter percentage of 50 percent in the diffusion space to avoid further partial voluming . The ROIs defined on the structural images are now transformed into the DTI space and thresholded based on the thresholded white matter partial volume map in the diffusion space. This would ensure that the ROIs are located within the white matter of the diffusion anisotropy image and would prevent any erroneous calculations. The ROIs are visually inspected to ensure that the ROIs are within the white matter of the FA image (Figure16 and

Figure17). The mean FA is calculated from the seven different segments of the corpus callosum. Similarly the mean DTI metrics like mean diffusivity (MD is calculated by overlaying the ROIs on the respective images). Measurements pertaining to diffusivity provide information about the amount of diffusion at a particular voxel in the image. For example, mean diffusivity is a measure of the average value of diffusion at a particular voxel. FA and ADC are inversely related; FA decreases when the value of diffusion at a particular voxel increases. ROIs which were initially drawn on a voxel thick sagittal slice are extended one voxel to the left and one voxel to the right making the ROI three voxels thick. Mean DTI metrics were calculated from these ROIs. Results of ROI analysis are summarized in detail in the results section.

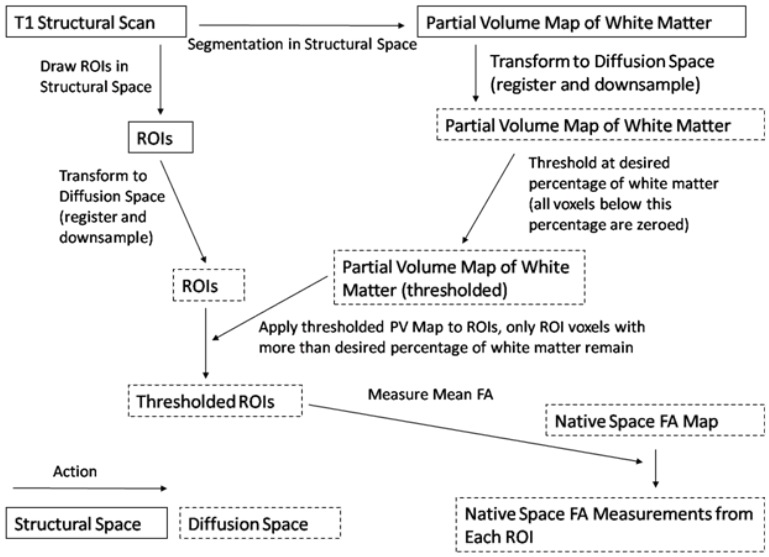

Figure 15: Flow shart describing the steps employed for the ROI analysis

2.7 Tract Based Spatial Statistics Analysis

Tract-based spatial statistics (TBSS) (Smith et al., 2006) is a method distributed under the FSL package for multi-subject analysis of diffusion anisotropy. Fractional anisotropy (FA), a quantitative measure of diffusion anisotropy is a straightforward measure for comparisons across subjects. It can be used across subjects since it is a scalar value measured at each voxel and is independent of the fiber orientation. The

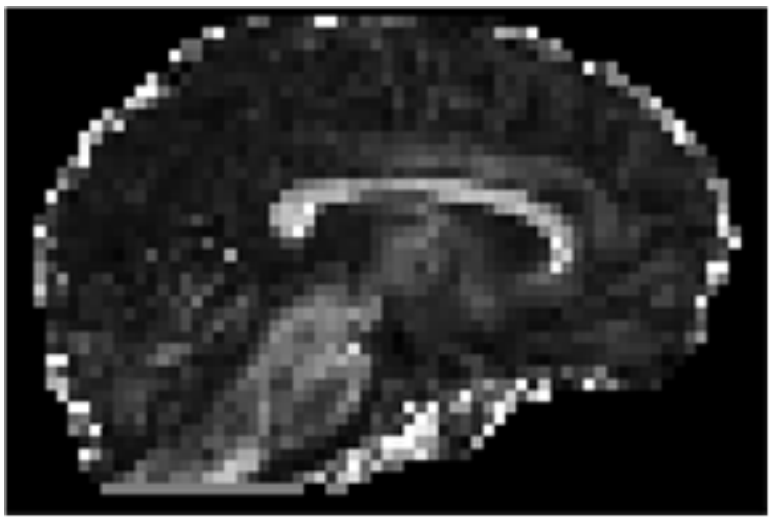

Figure 16: Fractional Anisotropy image

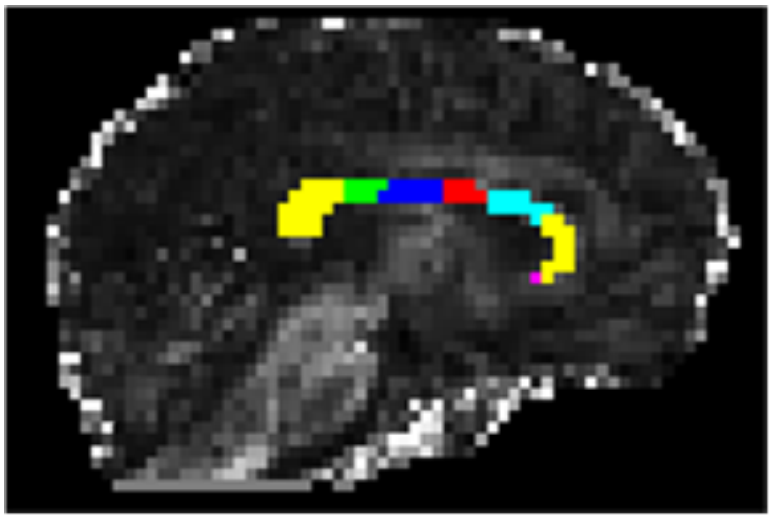

Figure 17: Corpus callosum ROIs overlayed on the FA image

efficacy of the multi-subject analysis is compromised by the use of standard registration algorithms. Also, the extent to which spatial smoothing is used, which leads to partial voluming, is one of the main concerns. Most of the VBM [Ashburner and Friston, 2000, Good et al., 2001] style FA analysis aligns each subjects FA images to a template. Then the voxel-wise statistics are carried out to find areas which correlate with the covariate of interest. As mentioned above, the main concern would be effective registration (how well a voxel in the standard space is registered to the corresponding voxel in the subject's FA image) and the extent to which spatial smoothing is used. These issues are addressed in this method by projecting individual subjects' FA data into a common space such that they are not dependent on perfect nonlinear registration. This is achieved through the use of an initial approximate nonlinear registration, followed by projection onto an alignment-invariant tract representation (the "mean FA skeleton"). No spatial smoothing is necessary in the image processing.

The method consists of five major steps:

2.7.1 Preparing the FA images

Fractional anisotropy (FA) images were created by fitting the diffusion tensor to the raw diffusion data. The raw diffusion data were corrected for subject movement, eddy currents, and distortion due to susceptibility artifact during the pre-processing step. A brain mask is created from one of the images without diffusion weighting (B=0) and the diffusion tensor model is fit to the raw diffusion data. Each subject's FA image is copied into a TBSS working directory, giving each subject's FA image a different name. This is the directory where the subsequent TBSS analysis is run. In the first step, the FA images are eroded and the end slices are removed to correct for any outliers that arose during diffusion tensor fitting. This step creates a new directory called FAi where all the registration steps take place and a directory for storing the original images.

2.7.2 Registration step

During the next step, all FA images are nonlinearly aligned to a standard space image or any other target image. The target image can be a pre-defined target or a group-wise, minimal- deformation target (MDT) brain. The option with a group-wise, MDT brain is recommended if interested in generating a study specific template and registering to an adult human derived FA target template is not a appropriate option. The group's MDT brain is identified by warping all individual brain images in the group to each other . FMRIB‘s non-linear registration tool called FNIRT is used for non-linear warping.

2.7.3 Post Registration step

In the third step, the non-linear transforms formed in the previous stage are used to move all the subjects' images to a standard space. MDT is selected as an image that minimizes the amount of required deformation from other images in the group. Once the MDT brain is selected, all images in the group are normalized using this brain as a target. Then, the target image is affine registered to a standard space template (chimp template (Figure 19). A cohort-specific template was derived using the subjects FA images. First, a template FA image is chosen from the group whose gravity center is properly centered at the junction of fornix and the corpus callosum. Then each subject‘s FA image is registered to this template using rigid body registration and averaged. This step creates a rigid body registration template for the group of subjects. In the next step, each subject‘s FA image is registered to the rigid body template using affine registration and averaged. This step creates an affine registration template. In the last step, each subject‘s FA image is registered to the affine registration template using non-linear registration and averaged creating a template which is symmetric and more reliable. Later, all the other subjects are moved to standard space by combining the non-linear transform to the target and

the affine transformation from target to standard space. The standard space has a higher resolution than the diffusion anisotropy images. This difference in resolution helps to avoid significant interpolation blurring (i.e., increase in partial voluming) when the nonlinear warp plus standard-space affine transformation is applied to each individual subject's data.

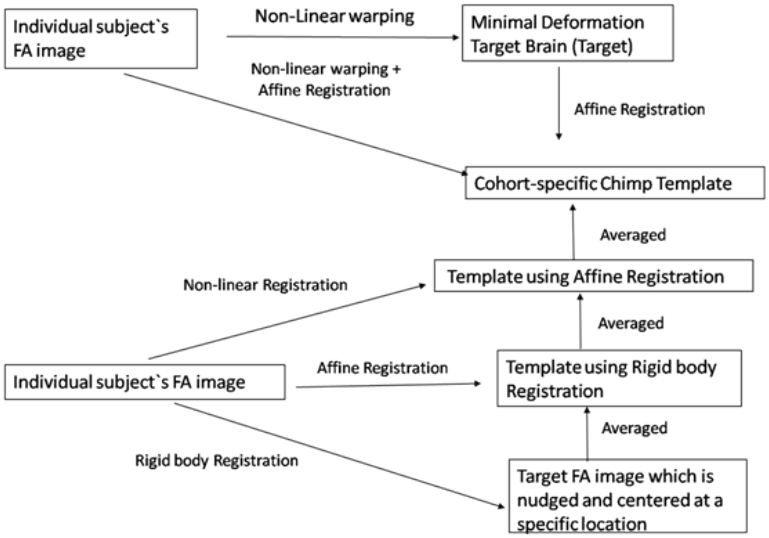

Figure 18: Flow chart describing the steps followed for moving all the FA images into standard space. Steps employed for generating a standard space chimpanzee template is also shown.

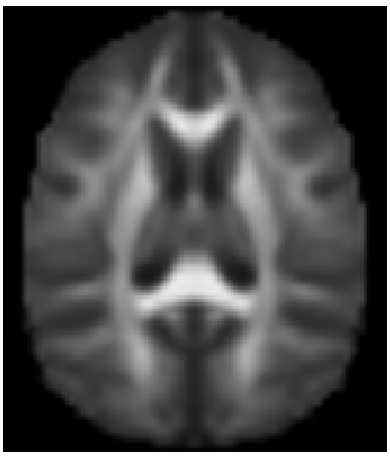

Figure 19: Cohort-specfic FA template derived from a group of 21 female chimpanzees.

2.7.4 Pre-statistics step

In this step, individual FA images are averaged to produce a mean anisotropy image (Figure 21) for the group. The mean FA image is relatively smooth (Figure20) due to effective averaging of the FA images and also due to resolution up sampling. This image is used to create a group-wise skeleton (Figure21) of white matter tracts. The skeletonization procedure is a morphological operation, which extracts the medial axis of an object. This procedure is used to encode the medial trajectory of the white matter fiber tracts with one-voxel thin sheaths. The mean FA skeleton is thresholded at 0.2 to remove cross-subject variability and to compensate for instances in which the nonlinear registration has not been able to attain good alignments.

Finally, FA images are projected onto the group-wise skeleton of white matter. This step compensates for the residual misalignment among individual white matter tracts. For individual images, FA values are analyzed along the normal projection for each point of the skeleton image and a peak value is assigned to the skeleton. The FA values vary rapidly perpendicular to the tract direction, but vary slowly along the tract direction. By assigning the peak value to the skeleton, this procedure effectively lines up the center of individual white matter tracts. This step effectively corrects for misalignment of individual fiber tracts. The projection operation is performed under two conditions: A distance map is created from the skeleton mask to establish search borders for individual tracts. The borders are created by equally dividing the distance between two nearby tracts. Secondly, a multiplicative 20-mm full width at half-max Gaussian weighting is applied during the search to limit the maximum projection distance from the skeleton. For each subject, filled the skeleton with FA values from the centers of the nearest relevant tracts. The skeletonized FA (4D) image is shown in the figure (fig5) below. Therefore for each subject the skeleton is filled with FA values from the centers of the nearest relevant tracts.

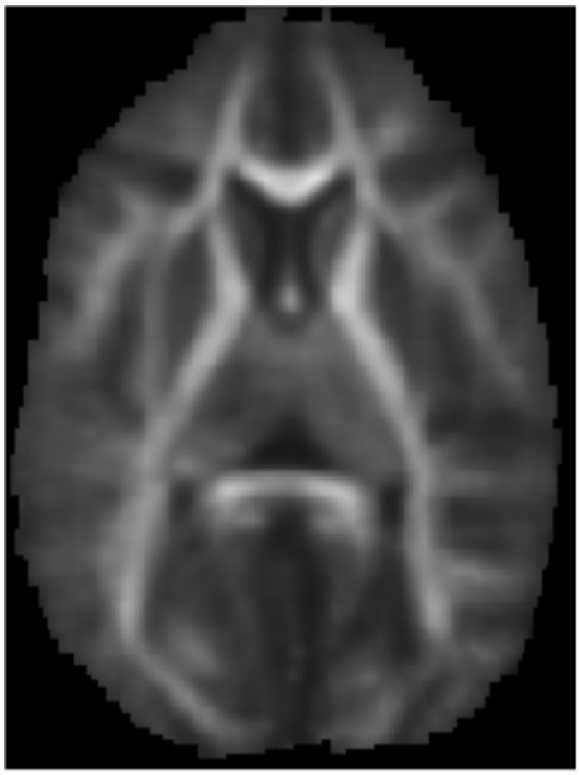

Figure 20: Mean FA image

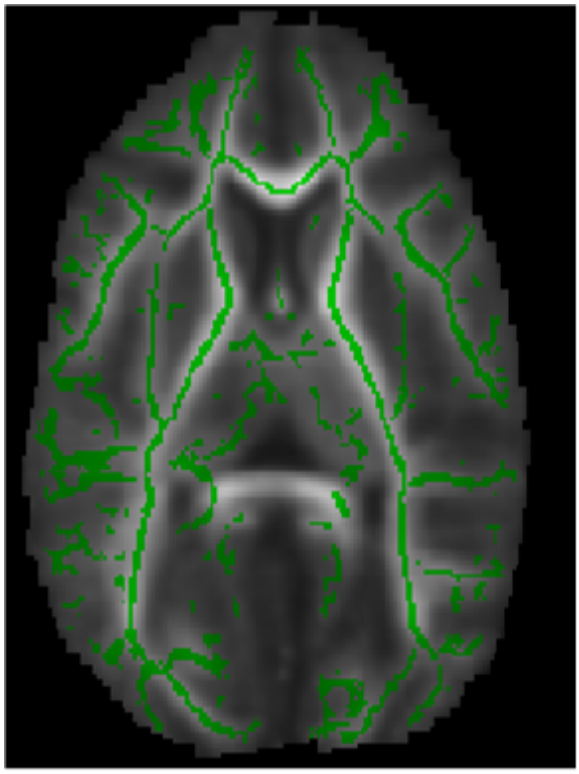

Figure 21: Skeltonized (4D) file showing the tracts on the mean FA image

2.7.5 Voxel wise statistics on the Skeletonized FA data

Voxel wise statistics aiming at any group differences or correlation of FA skeleton voxels with a covariate (example, age) are carried out on the skeletonized FA image. Statistics in TBSS are performed using the "Randomise" tool. Randomise uses a general linear model and contrasts to test effects of interest with different statistical measures. Before running Randomise a design matrix and a design contrast file using the Glm (Figure22) tool has to be created. Since the variation of FA with age, the covariate would be age. We need to demean (remove the mean) both the data and the covariate before running the Randomise. Assuming that the vector y is the covariate, calculating y -mean(y), gives the demeaned covariate.

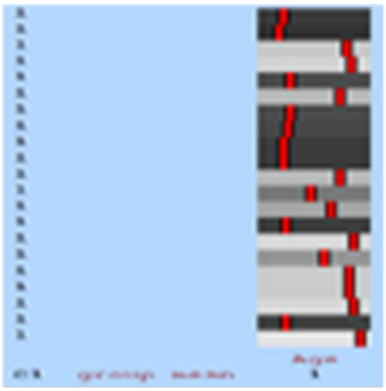

Figure 22: Figure shows the design matrix file setup using the demeaned covariate (i.e. age)

The demeaned covariate was provided as the design matrix file and then a default value of 5000 generic permutations were performed on this matrix. The order of entry of rows in the design matrix file should match with the alphabetical order of the original FA images, as that determines the order of the aligned FA images in the final 4D skeletonized FA file. The output of Randomise would be a t-statistic image and a p-value image corresponding to the t-statistic (Figure23). Thresholding at a p value of 0.05 would give significant clusters corresponding to the highly correlated voxels in the skeleton. For convenience 1-p is actually displayed, so thresholding at

.95 gives significant clusters (Figure24).

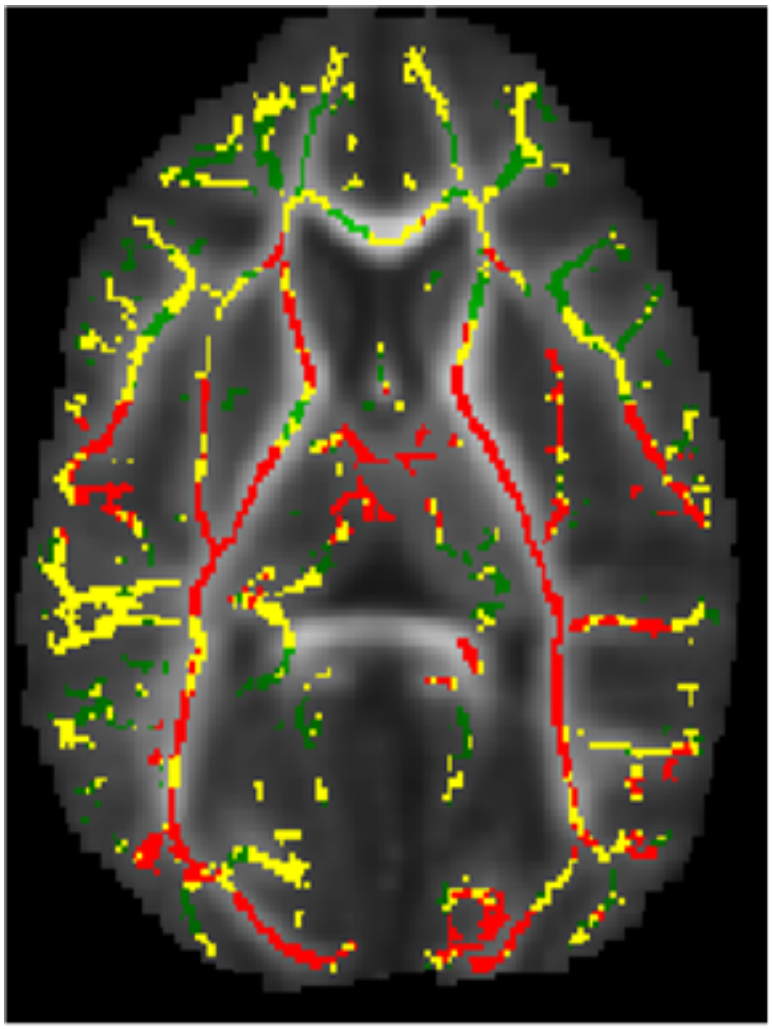

Figure 23: shows the voxel-wise t-statistic map highlighting the clusters with significant correlations between the data and the covariate. Significant clusters are highlighted in red-yellow.

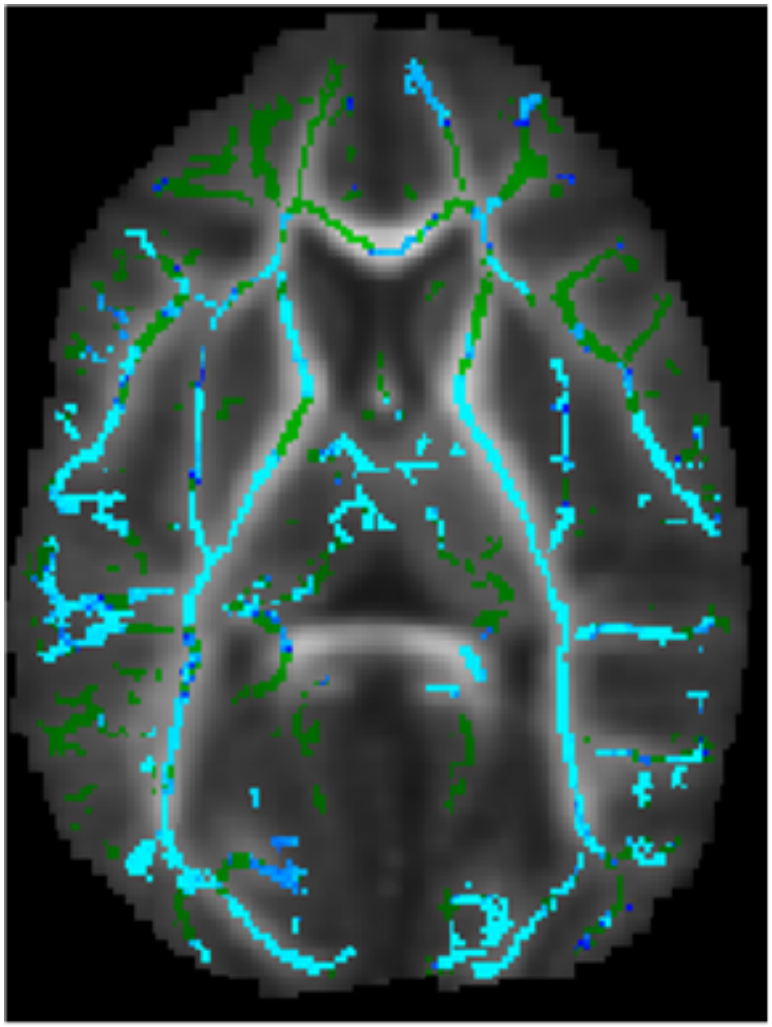

Figure 24: Figure shows the p-value map corresponding to the t-statistic map. Significant clusters thresholded at 0.95(1-p) are shown in blue-lightblue.

CHAPTER III

RESULTS

3.1 Region of Interest Analysis

Mean Fractional Anisotropy (FA) was calculated from the regions of interest defined in the corpus callosum (CC) using the methods mentioned in the analysis section. FA values varied considerably across the corpus callosum for all 21 subjects (Figure25), ranging from .53 in posterior midbody to .65 in splenium. The FA values from the rostrum were very low compared to the other regions due to partial voluming. The values of FA across the corpus callosum seem to high compared with humans(Figure25). The trend of change is almost similar ignoring the values from rostrum(due to partial voluming).

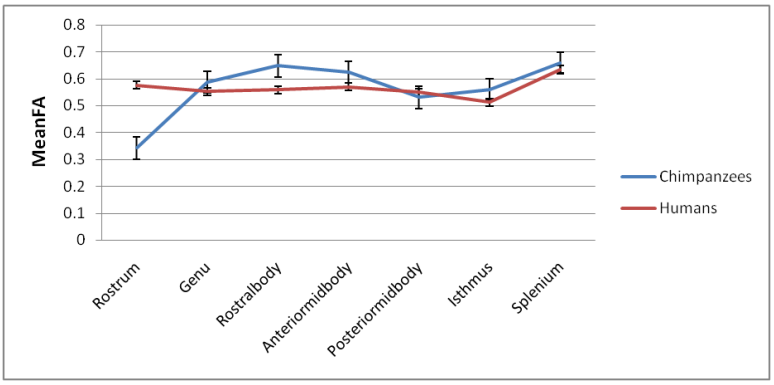

Figure 25: Variation of FA values across corpus callosum for the group of 21 chimpanzees

3.2 Correlations of FA with age

Across all 21 subjects, FA from all the regions of corpus callosum positively correlated with age (Figure26). Correlations were almost significant for posterior mid-body (r =.386, p=.072) and isthmus (r =.426, p=.054). The results indicate an increase

in white matter structural integrity with age in chimpanzees, contrary to what is observed in humans.

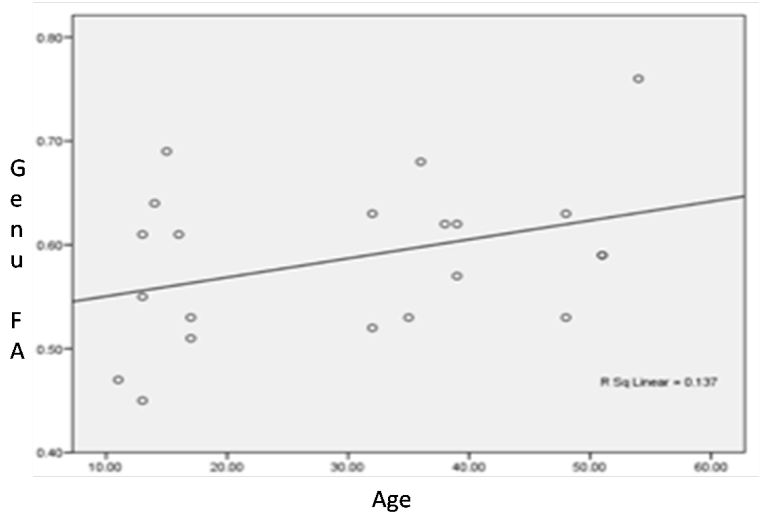

Figure 26: Correlation of FA with age in the genu. A positive correlation(not significant)is observed.

In addition, regional ADC significantly decreased with age in the genu (r = -.535, p= .013), rostral body (r= -.510, p=.018), posterior mid- body (r=.559 , p=.008), isthmus (r= -.588, p=.005) , splenium (r=.619 , p=.003) (Figure27). Across all the subjects, ADC and FA were highly, inversely correlated(r=-.633,p=.0037).

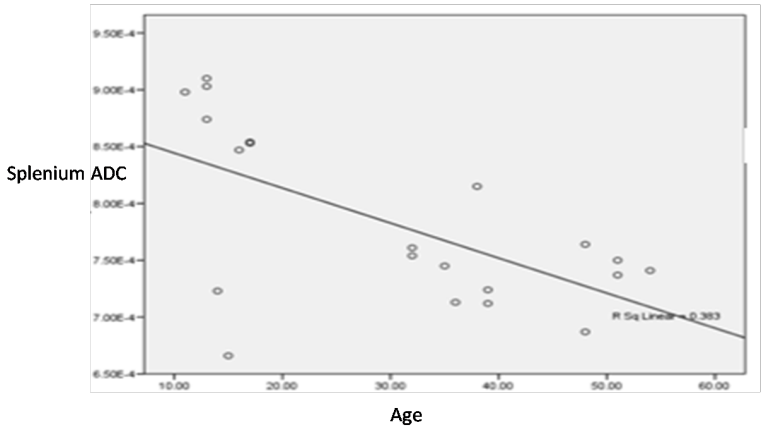

Figure 27: Correlation of ADC with age in the splenium. A negative correlation(significant)is observed.

3.2.1 Mean FA across the Age-Groups

Figure28 below shows the differences in the values of Mean FA across the corpus callosum for different age-groups. The age groups were young (10-20 years), old (30-40 years) and very old (40 and older). The figure indicates that the mean FA across corpus callosum increases from the young age group to the very old age group. The trend of change in the mean FA values across the corpus callosum is similar for all the age-groups.

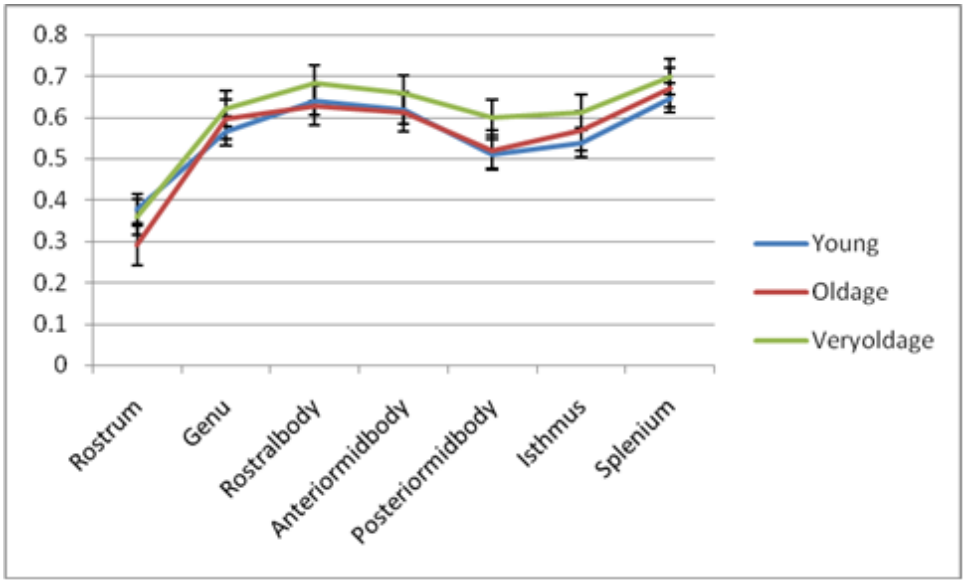

Figure 28: Trend of change in mean FA across the age-groups(Young,old,very old

3.2.2 TBSS Analysis

Voxel wise correlations between CC FA values and age were carried out on the group of 21 chimpanzees using Tract Based Spatial Statistics (TBSS). Voxel wise statistics were calculated using a randomise tool that performed a generic permuation test with 500 permuations. Output included the t-statistic map and a p-value map highlighting the clusters with significant correlations between the CC FA values and the covariate used (age). Results showed significant correlations between the CC FA values and age throughout the corpus callosum when a postive contrast was used, i.e.

positive correlation between FA and age. Tract based ROI analysis was performed on the white matter tracts with in the corpus callosum following the witelson convention. Results show a positive correlation between the FA values and age across the corpus callosum for all the 21 subjects,except for rostral body(r=-.074,p=.751). Correlations were significant for isthmus (r= .649,p=.001)and posterior midbody (r=.526,p=0.014). TBSS results are also in accordance with the ROI analysis results indicating an increase in the white matter structural integrity with age across the group of 21 chimpanzees. (Figure29) below compares the mean FA obtained using the ROI analysis and TBSS tracts based ROI analysis across the corpus callosum. Mean FA values are high using TBSS analysis since they are calculated along the center of the tracts within the regions of interest.

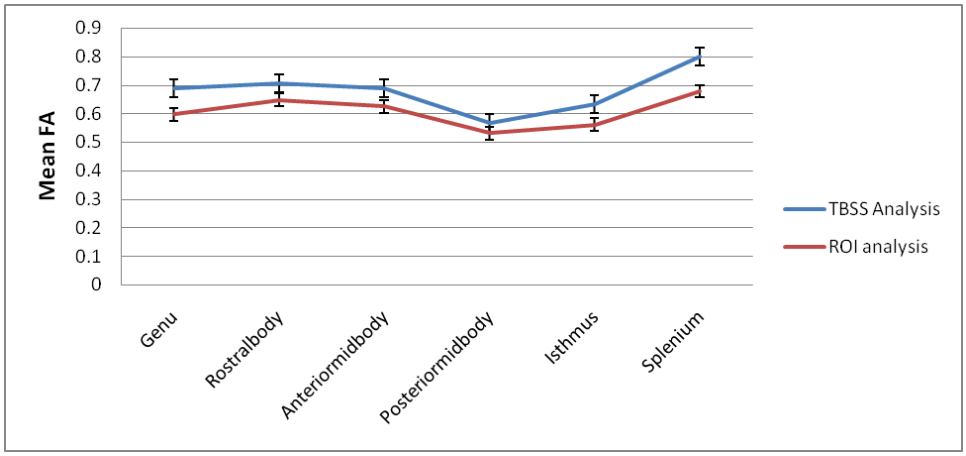

Figure 29: Trend of change in mean FA across the corpus callosum using ROI analysis and TBSS tract based ROI analysis. A similar trend of change in mean FA is observed across the corpus callosum using both the methods.

CHAPTER IV

DISCUSSION

The results from the ROI analysis and TBSS analysis show that the FA values across the corpus callosum in chimpanzees increase with age, but were not highly significant. This finding indicates an age-related increase in the white matter structural integrity, which is contrary to the evidence of age-related decreases in whitematter FA in humans. Based on the little evidence available about the changes in white matter microstructure with age in chimpanzees, results from the two different analyses can give rise to two possible conclusions: there is a true increase in the white matter structural integrity with age in chimpanzees or the results are erroneous, due to various reasons. Possible causes for erroneous results might be the influence of low SNR due to ghosting artifacts on the calculated DTI metrics.

4.1 Influence of Ghosting on the measured FA

Ghosting caused by cardiac pulsation artifacts is observed to be a potential problem affecting DTI calculations in chimpanzees. Ghosting caused the appearance of signal outside the brain (a well known ghosting pattern), but also a loss of signal from within the brain. This loss of signal leads to a poorer SNR within the brain. Poor SNR has a significant effect on the measured DTI metrics. When the true FA is closer to zero, (i.e. in CSF) noise will cause the FA values to deviate from zero in the positive direction, i.e to overestimate FA. When the true FA is closer to 1, noise will cause the values to deviate from 1 in the negative direction, i.e to underestimate FA. Between these two extremes, there is a continuum for different values of FA. Also, it has been observed that the effects of ghosting significantly decrease with the age and weight of the chimpanzees. If chimpanzees follow the trend observed in humans,

then younger chimpanzees should theoretically have higher FA in the corpus callosum than the older ones, and FA is being extremely underestimated in our sample. This underestimation might be an important reason for the increase in FA values with age observed in the chimpanzees.

A measure of the ghosting signal from the DTI images was made by drawing an ROI out side and 8mm below the gravity center of the brain (near the temporal lobe)(Figure30), where ghosting is observed to be maximal across the group.

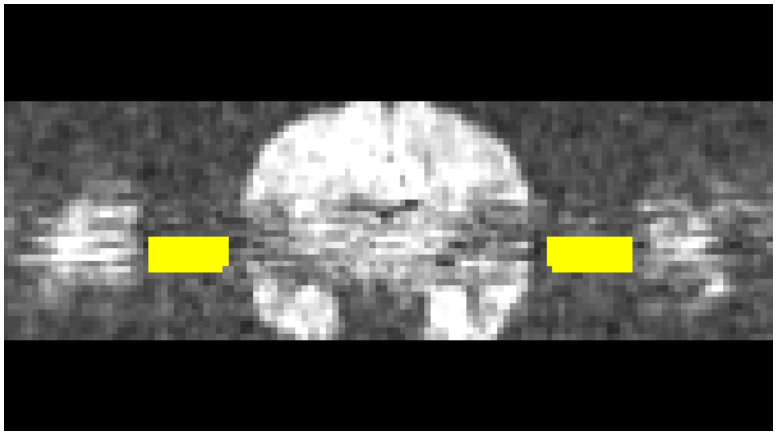

Figure 30: ROI drawn to measure the signal due to ghosting where it is observed to be maximal across the group.ROI is drawn outside and 8mm below the gravity center of the brain

The background signal has to be removed from the measured ROI signal to obtain a pure estimate of the signal due to ghosting free from the background noise. Instead, of directly subtracting the background signal from the Measured ROI signal, the ghosting signal, free from noise, was estimated using the relationship:

$$M = \sqrt{(A^2 + \sigma^2)} \tag{2}$$

(Hakon Gudbjartsson., et al., MRM, 1995, 34, 910)

Where, A is the ghosting signal free from background noise, M is the measured signal combined with background noise and σ is the standard deviation of the original complex image (equal to standard deviation of the Measured signal when the signal

is dominant). σ can be estimated from the mean of the background noise based on the relationship: mean of background noise (no signal) $= 1.25 * \sigma$ (Appendix B, relationship B.21, Haacke et al.Magnetic Resonance Imaging: Physical Principles and Sequence Design). Hence, the Ghosting signal free from noise was estimated by

$$A = \sqrt{(M^2 - \sigma^2)} \tag{3}$$

The amount of ghosting signigicantly decreased with age(r=.8515,p=.001)(Figure31). Correlations between the amount of ghosting signal and mean FA are negative and are marginally siginficant across the corpus callosum (Genu(r=-.320,p=.154)(Figure32). After controlling for ghosting, partial correlations between age and FA are still positive but not highly significant(genu(r=.187,p=.430).

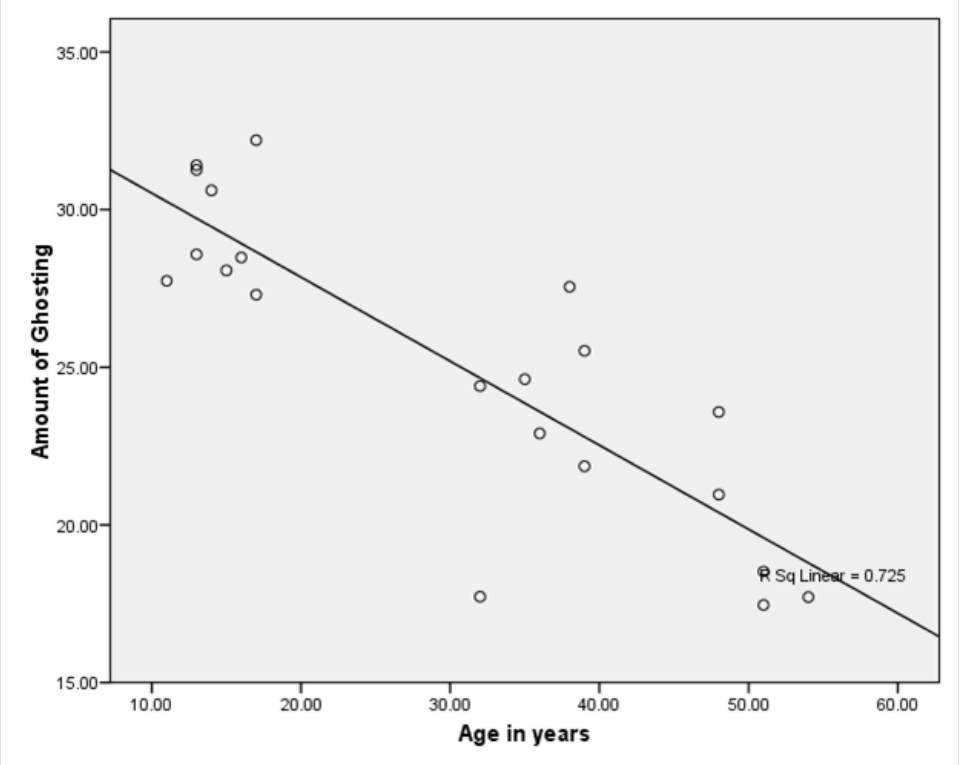

Figure 31: Significant negative correlation between age and amount of ghosting signal for all the 21 chimpanzees.

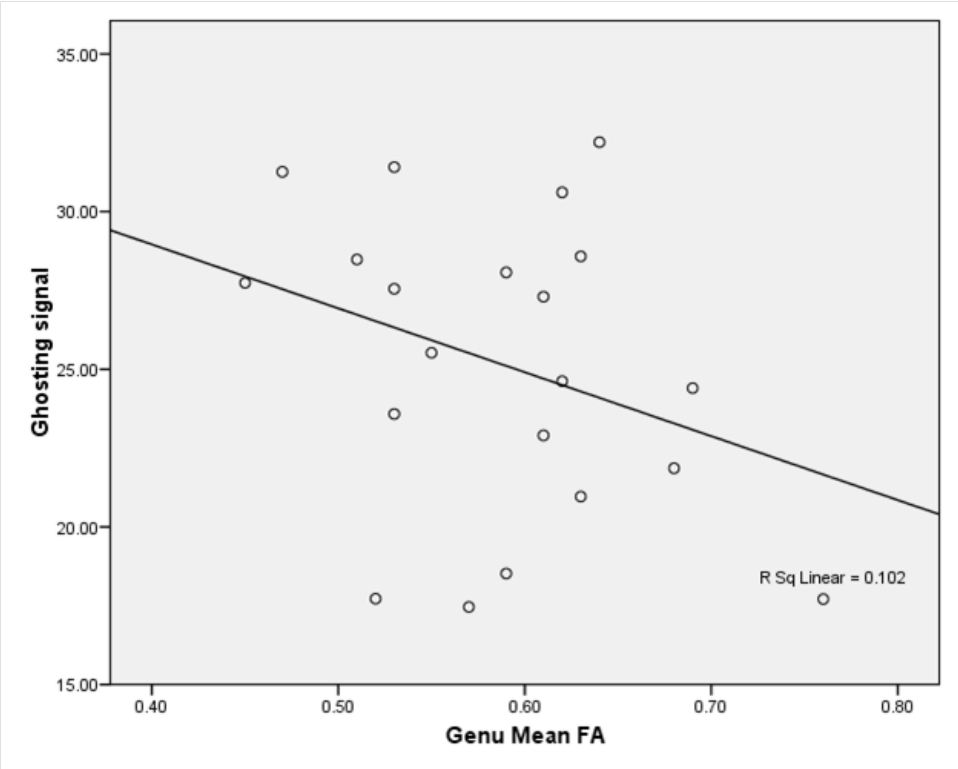

Figure 32: Marginal negative correlation between genu mean FA and amount of ghosting signal for all the 21 chimpanzees.

4.2 FA Simulations considering the effects of Ghosting

Simulations of FA under the influence of the ghosting signal were performed using the method proposed by C.G.Koay et al (2006). The ghosting signal free from noise was measured for all 60 directions and provided input noise for the simulations. The direction-dependent noise variance was taken into account in the diffusion tensor estimation. The simulations of the FA values were performed considering the effects of the ghosting signal for each diffusion weighted direction independently. The simulated FA values for an old chimpanzee (51 years) and a young chimpanzee (17 years) were compared in the figures (Figure33 and Figure34) below. The red line indicates the standard FA values ranging from 0.1 to 1. The black line indicates the simulated FA under the influence of ghosting.

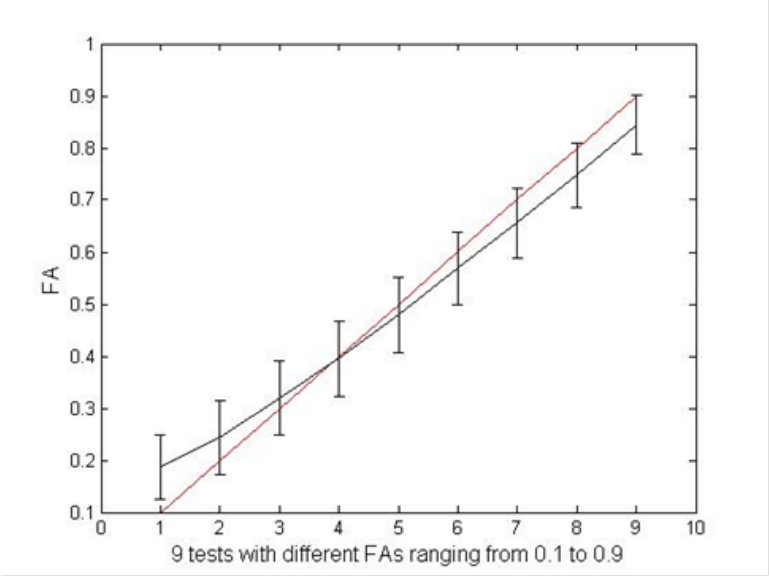

Figure 33: Figure explains the variation of the simulated FA under the influence of ghosting (black line) compared with the reference (red line) for an old chimpanzee. It is clearly seen that the ghosting underestimates FA at larger FA values and overestimates it at lower FA values. The difference is proportional to the amount of ghosting in the subject.

It is clearly observed that the increase in the mean of the ghosting signal (17 units for the old chimpanzee and 34 units for the younger one) increased the difference

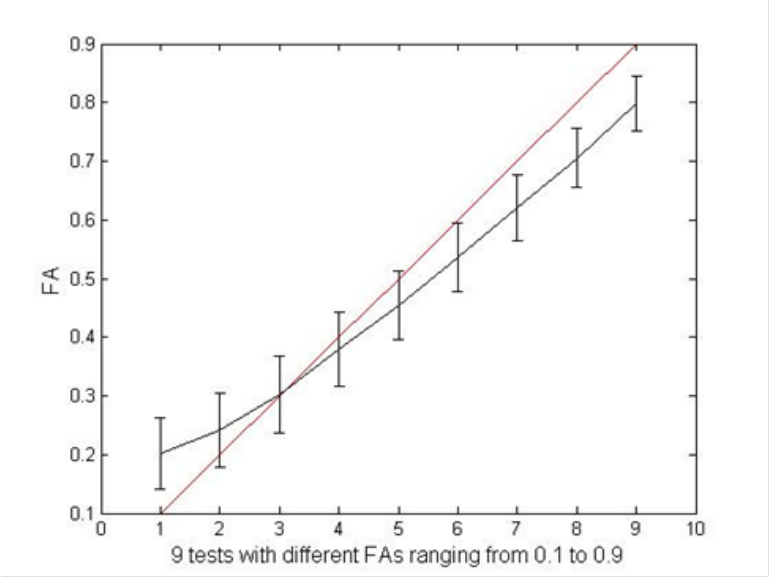

Figure 34: Figure explains the variation of the simulated FA under the influence of ghosting (black line) compared with the reference (red line) for a young chimpanzee. The difference is proportional to the amount of ghosting in the subject and is high due to large amount of ghosting in a younger chimpanzee compared to an older one.

between standard and measured FA values. Therefore, the mean FA for younger chimpanzees is underestimated to a larger extent compared to older chimpanzees. This might be the potential cause for decrease in FA values for younger chimpanzees.

Our overall findings suggest that FA increases with age in chimpazees. This trend can potentially be explained by physiological aging or the effects of ghosting on the measured DTI metrics. The combination of findings in human literature, which suggest an decrease in FA with age with the results presented in the previous sections of this study lead ghosting to be the favored explaination for the observed trends. However,the more effective methods for estimating the true FA need to be further researched. Based on the results from the simulations, future work aims at developing a method for back-projecting the FA values based on the amount of ghosting present in the chimpanzee.

CHAPTER V

REFERENCES

1. Basser PJ. Inferring microstructural features and the physiological state of tissues from diffusion-weighted images. NMR Biomed 1995; 8:333-344.

2. Pierpaoli C, Basser PJ. Toward a quantitative assessment of diffusion anisotropy. Magn Reson Med 1996; 36:893-906.

3. Beaulieu C. The basis of anisotropic water diffusion in the nervous system: a technical review. NMR Biomed 2002; 15:435-455

4. Pfefferbaum, A., Sullivan, E.V., 2003. Increased brain white matterdiffusivity in normal adult aging: relationship to anisotropy and partialvoluming. Magnetic Resonance in Medicine 49, 953-961.

5. Pfefferbaum, A., Sullivan, E.V., Hedehus, M., Lim, K.O., Adalsteinsson, E., Moseley, M., 2000a. Age-related decline in brain white matteranisotropy measured with spatially corrected echo-planar diffusion tensor imaging. Magnetic Resonance in Medicine 44, 259-268.

6. O'Sullivan, M., Jones, D., Summers, P., Morris, R., Williams, S., Markus, H., 2001. Evidence for cortical "disconnection" as a mechanism of age-related cognitive decline. Neurology 57, 632-638.

7. Chun, T., Filippi, C.G., Zimmerman, R.D., Ulug, A.M., 2000. Diffusion changes in the aging human brain. American Journal of Neuroradiology 21, 1078-1083.

8. Madden, D.J., Whiting, W.L., Huettel, S.A., White, L.E., MacFall, J.R.,Provenzale, J.M., 2004. Diffusion tensor imaging of adult age differences in cerebral white matter: relation to response time. Neuroimage 21, 1174-1181.

9. Nusbaum, A.O., Tang, C.Y., Buchsbaum, M.S., Wei, T.C., Atlas, S.W.,2001. Regional and global changes in cerebral diffusion with normal aging. American Journal of Neuroradiology 22, 136-142.

10. Stebbins, G., Carrillo, M.D., Medina, D., de Toledo-Morrell, L., Klingberg, T., Poldrack, R.A., Moseley, M., Karni, O., Wilson, R.S., Bennett, D.A., Gabrieli, J.D.E., 2001. Frontal white matter integrity in aging and its relation to reasoning performance: a diffusion tensor imaging study (abs 456.3). Society for Neuroscience Abstracts 27, 1204.

11. Sullivan, E.V., Rosenbloom, M.J., Serventi, K.L., Pfefferbaum, A., 2004.Effects of age and sex on volumes of the thalamus, pons, and cortex. Neurobiology and Aging 25, 185-192.

12. Blatter, D.D., Bigler, E.D., Gale, S.D., Johnson, S.C., Anderson,C., Burnett, B.M., Parker, N., Kurth, S., Horn, S., 1995. Quantitative volumetric analysis of brain MRI: normative database spanning five decades of life. American Journal of Neuroradiology 16, 241-245.

13. Guttmann, C.R.G., Jolesz, F.A., Kikinis, R., Killiany, R.J., Moss, M.B., Sandor, T., Albert, M.S., 1998. White matter changes with normal aging. Neurology 50, 972-978.

14. Beal MF. 1995. Aging, energy, and oxidative stress in neurodegenerative diseases. Ann Neurol 38(3):357-66.

15. Helenius J, Soinne L, Salonen O, Kaste M, Tatlisumak T. 2002. Leukoaraiosis, ischemic stroke, and normal white matter on diffusion-weighted MRI. Stroke 33(1):45-50.

16. Raz N, Torres IJ, Spencer WD, Acker JD. Pathoclysis in aging human cerebral cortex: evidence from in vivo MRI morphometry. Psychobiology 1993;21:151-160.

17. Rakic P, Yakovlev P. Development of the corpus callosum and cavum septi in man. J Compar Neurol 1968;26:100-104.

18. Sullivan, E.V., Deshmukh, A., Desmond, J.E., Lim, K.O., Pfefferbaum,A., 2000. Cerebellar volume decline in normal aging, alcoholism, and Korsakoff's syndrome: relation to ataxia. Neuropsychology 14,341-352.

19. K.M. Hasan, R.K. Gupta, R.M. Santos, J.S.Wolinsky, P.A. Narayana, Diffusion tensor fractional anisotropy of the normal-appearing seven segments of the corpus callosum in healthy adults and relapsing-remitting multiple sclerosis patients, J. Magn. Reson. Imag. 21 (2005) 735-743.

20. H. Huang, J. Zhang, H. Jiang, S.Wakana, L. Poetscher, M.I. Miller, P.C.M. van Zijl, A.E. Hillis, R. Wytik, S. Mori, DTI tractography based parcellation of white matter: application of the mid-sagittal morphology of corpus callosum, Neuroimage 26 (2005) 295-305.

21. M. Ota, T. Obata, Y. Akine, H. Ito, H. Hiroo, T. Asada, T. Suhara, Agerelated degeneration of corpus callosum measured with diffusion tensor imaging, Neuroimage 31 (2006) 1445-1452.

22. S.F. Witelson, Hand and sex differences in the isthmus and genu of the human corpus callosum, Brain 112 (1989) 799-835.

23. Charlton, R.A.; Barrick, T.R.; McIntyre, D.J.; Shen, Y.; O'Sullivan, M.; Howe, F.A.; Clark, C.A.; Morris, R.G.; Markus, H.S. White matter damage on diffusion tensor imaging correlates with age-related cognitive decline. Neurology. 2006;66:217-222.

24. Herndon JG, Tigges J, Klumpp SA, Anderson DC (1998a) Brain weight does not decrease with age in adult rhesus monkeys. Neurobiol Aging 19:267-272.

25. Herndon JG, Tigges J, Anderson DC, Klumpp SA, McClure HM. 1999. Brain weight throughout the life span of the chimpanzee. J Comp Neurol 409(4):567-572.

26. Andersen AH, Zhang Z, Zhang M, Gash DM, Avison MJ. 1999. Age-associated changes in rhesus CNS composition identified by MRI. Brain Res 829(1-2):90-98.

27. Lyons DM, Yang C, Eliez S, Reiss AL, Schatzberg AF. 2004. Cognitive correlates of white matter growth and stress hormones in female squirrel monkey adults. J Neurosci 24(14):3655-3662.

28. Lacreuse A, Diehl MM, Goh MY, Hall MJ, Volk AM, Chhabra RK, Herndon JG. 2005. Sex differences in agerelated motor slowing in the rhesus monkey: behavioral and neuroimaging data. Neurobiol Aging 26(4):543-551.

29. Feldman ML, Peters A. 1998. Ballooning of myelin sheaths in normally aged macaques. J Neurocytol27(8):605-614.

30. Peters A, Moss MB, Sethares C. 2000. Effects of aging on myelinated nerve fibers in monkey primary visual cortex. J Comp Neurol 419(3):364-376.

31. Peters A, Sethares C. 2002. Aging and the myelinated fibers in prefrontal cortex and corpus callosum of the monkey. J Comp Neurol 442(3):277-291.

32. Jones DK, Horsfield MA, Simmons A (1999) Optimal strategies for measuring diffusion in anisotropic systems by magnetic resonance imaging. Magn Reson Med 42:515-525.

33. Bowtell, R., McIntyre, D.J.O., Commandre, M.-J., Glover, P.M., Mansfield,P., 1994. Correction of geometric distortion in echo planar images. Proceedings of the 2nd Meeting of the Society of Magnetic Resonance, p. 411.

34. Jesper L.R. Andersson, Stefan Skare, John Ashburner .How to correct susceptibility distortions in spin-echo echo-planar images:application to diffusion tensor imaging. NeuroImage 20 (2003) 870-888.

35. P. Kochunov, P.M. Thompson, J.L. Lancaster, G. Bartzokis, S. Smith,T. Coyle, D.R. Royall, A. Laird, and P.T. Fox .Relationship between white matter fractional anisotropy and other indices of cerebral health in normal aging: Tract-based spatial statistics study of aging. NeuroImage 35 (2007) 478-487.

36. Y. Zhang, M. Brady, and S. Smith. Segmentation of brain MR images through a hidden Markov random field model and the expectation maximization algorithm.

IEEE Trans. on Medical Imaging, 20(1):45-57, 2001.

37. M. Jenkinson and S.M. Smith. A global optimisation method for robust affine registration of brain images. Medical Image Analysis, 5(2):143-156, June 2001.

38. Ashburner, J., Friston, K., 2000. Voxel-based morphometry-The methods. NeuroImage 11, 805-821.

39. Good, C., Johnsrude, I., Ashburner, J., Henson, R., Friston, K., Frackowiak, R., 2001. A voxel-based morphometric study of ageing in 465 normal adult human brains. NeuroImage 14 (1), 21- 36.

40. Hakon Gudbjartsson., et al., MRM, 1995, 34, 910.The Rician Distribution of Noisy MRI Data.

41. Koay, C.G., Chang, L.C., Carew, J.D., Pierpaoli, C., Basser, P.J., 2006. Aunifying theoretical and algorithmic framework for least squaresmethods of estimation in diffusion tensor imaging. J. Magn. Reson. 182 (1), 115-125.